Chinese Chemical Letters 37 (2026) 111012

Contents lists available at ScienceDirect

Chinese Chemical Letters

journal homepage: www.elsevier.com/locate/cclet

Size regulation from single-crystal to nanoscale of a polyoxometalate-based Cu-triazole complex for catalytic oxidation reaction of phenols

Yang Chu[a], Xiao-Hui Li[a,*], Zhong Zhang[a,b], Na Xu[a], Dan-Feng He[c], Xiu-Li Wang[a,*]

[a] College of Chemistry and Materials Engineering, Professional Technology Innovation Center of Liaoning Province for Conversion Materials of Solar Cell, Bohai University, Jinzhou 121013, China
[b] Key Laboratory of Advanced Energy Materials Chemistry (Ministry of Education), Nankai University, Tianjin 300071, China
[c] College of Science, Qiongtai Normal University, Haikou 571100, China

ARTICLE INFO

Article history:
Received 7 January 2025
Revised 5 February 2025
Accepted 26 February 2025
Available online 27 February 2025

Keywords:
Polyoxometalates
Cu-triazole complex
Size regulation
Synergistic catalysis
Oxidation reaction of phenols

ABSTRACT

Polyoxometalate-based metal-organic complexes (POMOCs) which combine the structural features and performance advantages of MOCs and POMs, have a wide application in the field of catalysis. However, the catalytic capacity of POMOCs commonly cannot be fully utilized due to their imporosity and low surface area of single-crystals. In this work, a new POMOC with a formula of $[Cu_3O(4\text{-atrz})_6(PO_3)(PMo_{12}O_{40})]$ (POMOC **1**, 4-atrz = 4-amino-4*H*-1,2,4-triazole) was synthesized. And the size regulation of POMOC **1** from single-crystal to nanoscale was achieved by using citric acid as a modulator and adjusting the reaction temperature. Nano-sized POMOC **1** exhibited excellent catalytic performance in the oxidation reaction of phenols owing to the synergistic catalysis of POM and coordinatively unsaturated Cu(II), and more surface-accessible catalytic sites of nano-catalyst.

© 2026 Published by Elsevier B.V. on behalf of Chinese Chemical Society and Institute of Materia Medica, Chinese Academy of Medical Sciences.

Polyoxometalates (POMs), as a kind of multi-nuclear metal-oxygen cluster anions with great redox properties and acidity, show excellent potential in the catalytic field [1–6]. However, the low surface area in non-polar solvent and high solubility in polar solvent of POMs limit their application in catalysis. Metal-organic complexes (MOCs) are a kind of crystalline materials constructed by the coordination between metal ions/clusters and ligands [7,8]. They have become one kind of the most popular heterogeneous catalysts because of their catalytic active sites of metals and ligands, structural diversity, and functional adaptability [9,10]. The combination of POMs and MOCs to form polyoxometalate-based metal-organic complexes (POMOCs) is an effective strategy to solve the aggregation and dissolution issues of POMs [11,12]. Furthermore, POM and metal sites in POMOCs may play synergistic catalysis, exhibiting higher catalytic activity in organic catalytic reactions [13–18]. N-containing ligands are commonly used to construct POMOCs by hydro/solvothermal methods, due to their abundant coordination modes [19,20]. However, these POMOCs frequently present nonporous structures, or pores of MOCs are occupied by POMs. Therefore, the catalytic activity of these POMOCs commonly cannot be fully utilized owing to little active sites exposing on the surface of large bulk crystals.

Reducing the size of POMOC crystals to nanoscale is an effective approach to improve their catalytic activity because of the higher specific surface area, more exposed active sites, and shorter reaction pathway of nano-crystals [21]. At present, researches on the nanocrystallization of coordination polymers mostly focus on pure porous metal-organic frameworks (MOFs). The main methods include coordination modulation [31–36], ultrasound assisted method [22,23], controlled reaction condition method [24–26], microemulsion method [27,28], microwave assisted method [29,30], *etc*. Among these methods, coordination modulation is a typical strategy to regulate the size and morphology of MOF crystals by the competition coordination of metal ions with organic ligands and modulators [31]. And different modulators have been introduced into the synthesis system of MOFs, including polymers [32], monodentate ligands [33,34], chelate ligands [35], surfactants [36]. However, the application of coordination modulation method for the system of POMOCs is rare, owing to the complicated synthesis system resulting from the introduction of POMs. Liu group used benzoic acid as the modulator to achieve the synthesis of submicron-sized NENU-3 with different morphology, which is composed of Cu(II) metal center, 1,3,5-benzenetricarboxylic acid ligand and $H_3PW_{12}O_{40}$ [37]. However, there are more complicated

* Corresponding authors.
E-mail addresses: lixh198@126.com (X.-H. Li), wangxiuli@bhu.edu.cn (X.-L. Wang).

https://doi.org/10.1016/j.cclet.2025.111012
1001-8417/© 2026 Published by Elsevier B.V. on behalf of Chinese Chemical Society and Institute of Materia Medica, Chinese Academy of Medical Sciences.

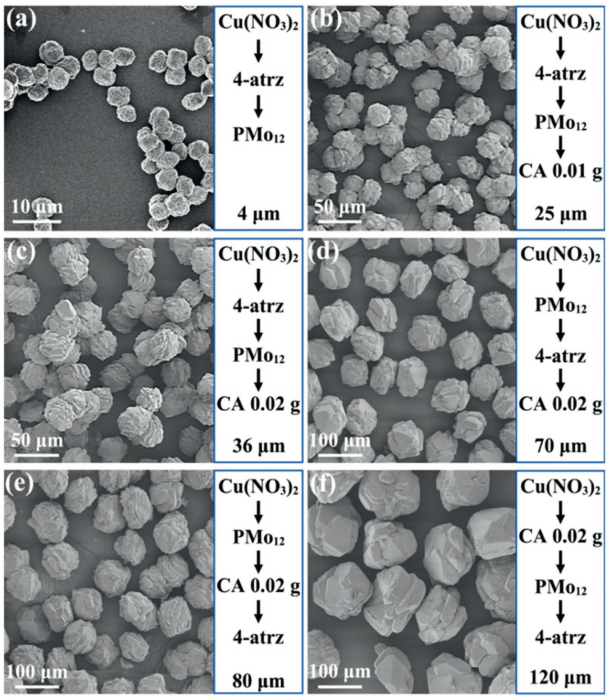


Fig. 1. SEM images of POMOC **1** prepared under different (a-c) dosage of CA and (d-f) feeding sequence.

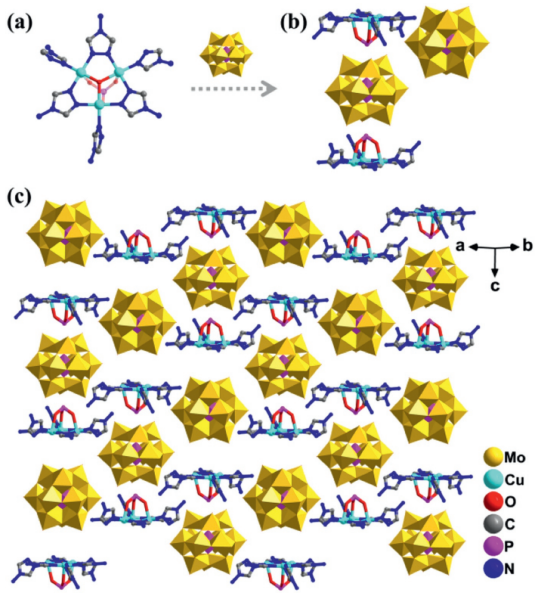


Fig. 2. The structure of (a) three-nucleated Cu cluster and (b) minimum repetition unit in POMOC **1**. (c) The 2D supermolecule structure of POMOC **1**. All H atoms were omitted for clarity.

interactions in the system of POMOCs with N-containing ligands, including coordination of metal-ligand, and electrostatic interaction between POM with ligand and metal. Therefore, it is a great challenge to produce pure phase nano-POMOC crystals with N-containing ligands.

In this work, $Cu(NO_3)_2$ and $H_3PMo_{12}O_{40}$ (PMo_{12}) with high activity in various catalytic reactions, and 4-amino-4*H*-1,2,4-triazole (4-atrz) with abundant coordination sites were selected as raw materials to research the size regulation of POMOC with N-containing ligand. A new POMOC, $[Cu_3O(4\text{-atrz})_6(PO_3)(PMo_{12}O_{40})]$ (POMOC **1**) was synthesized under hydrothermal conditions. And the size regulation of POMOC **1** from single-crystal to nano-crystal was achieved by citric acid (CA) as the coordination modulator and controlling reaction conditions. As-prepared nanoscale POMOC **1** exhibited excellent activity in the oxidation reaction of phenols to the corresponding *p*-benzoquinones (*p*-BQs).

Initially, the traditional hydrothermal method was attempted to prepare POMOC single-crystals by dissolving $Cu(NO_3)_2$, 4-atrz and PMo_{12} in water sequentially under stirring and then heating at 120 °C for 4 days. Unfortunately, green powder was obtained, which presented uniform block-shaped crystals with a size of 4 μm as demonstrated by scanning electron microscope (SEM) image (Fig. 1a). In order to determine the composition of this green powder, its infrared (IR) spectrum was compared with that of PMo_{12} and 4-atrz ligand (Fig. S1 in Supporting information). The characteristic peaks of PMo_{12} in 700–1100 cm^{-1} and the peaks of 4-atrz in 1190–1650 cm^{-1} and 2900–3500 cm^{-1} can be observed in the IR spectrum of the green powder, which proved the existence of POM and ligand [38]. Combining the above results with the color of crystals, it is speculated that obtained powder is the expected POMOC composed of Cu(II), 4-atrz and PMo_{12}, but has a small crystal size of 4 μm (denoted as **1**–4 μm). In order to obtain larger size of POMOC **1** crystals for single-crystal structure detection, coordination modulation method was used to slow down the reaction of Cu^{2+}, 4-atrz and PMo_{12}. CA was selected as the modulator based on the following points: (1) CA with multiple carboxylic and hydroxyl groups can form chelate with metal ions, thereby restraining the coordination of Cu^{2+} with 4-atrz and obtaining larger crystals; (2) CA is soluble in water and has no electrostatic interaction with POM, which will not introduce insoluble impurities into the reaction system. Different dosages of CA (0.01–0.03 g) were added to the above synthesized system of POMOC **1**–4 μm after adding PMo_{12}. When 0.01 g and 0.02 g of CA were added, the size of POMOC **1** increased to 25 μm (denoted as **1**–25 μm) and 36 μm (denoted as **1**–36 μm), respectively (Figs. 1b and c). When CA dosage increased to 0.03 g, impurity with different colors appeared, so 0.02 g CA was used for further exploration. Considering the coordination between Cu^{2+} with 4-atrz and CA, and the electrostatic interaction between PMo_{12} with Cu^{2+} and 4-atrz existing in the synthesized system of POMOC **1**, the feeding sequence may affect the size of POMOC **1** crystals. Therefore, feeding sequence of 4-atrz, PMo_{12} and CA were changed. When the sequence was changed to Cu^{2+}–PMo_{12}–4-atrz–CA (exchanging PMo_{12} and 4-atrz), the crystal size increased to 70 μm (denoted as **1**–70 μm, Fig. 1d). When the feed sequence was further changed to Cu^{2+}–PMo_{12}–CA–4-atrz, larger crystals of 80 μm were formed (denoted as **1**–80 μm, Fig. 1e). When the feeding sequence of Cu^{2+}–CA–PMo_{12}–4-atrz was selected, measurable single-crystal of POMOC **1** was obtained (denoted as **1**-SC), which showed a size of about 120 μm (Fig. 1f). Based on the above results, it can be found that the earlier Cu^{2+} reacts with 4-atrz, the smaller the crystal size; on the contrary, the earlier Cu^{2+} reacts with CA, the larger the crystal size.

A POMOC **1** single-crystal with suitable size and good shape was selected for single-crystal X-ray diffraction to detect its structure. The detailed crystallographic data of **1** were given in Tables S1 and S2 (Supporting information). It can be found that POMOC **1** belongs to the trigonal R-3 space group. POMOC **1** shows a zero-dimensional structure, in which the valence states of Cu, P and Mo are +2, +5 and +6, respectively, as determined by the X-ray photoelectron spectroscopy (XPS) of POMOC **1** (Fig. S2 in Supporting information). As shown in Fig. 2a, Cu(II) atoms in POMOC **1** are all five-coordinated. Each Cu(II) atom connects with three 4-atrz ligands, one μ_3-O atom, and one O atom from the PO_3 group to form a three-nucleated copper cluster $[Cu_3O(4\text{-atrz})_6(PO_3)]^{3+}$

(denoted as $\{Cu_3\}$). The $\{Cu_3\}$ clusters with positive charges combine with PMo_{12} anions by electrostatic interaction and hydrogen bonding to form the smallest repeating unit of POMOC **1** (Fig. 2b). Then these smallest repeating units extend into a 2D supermolecule layered structure by hydrogen bonding (Fig. 2c). The hydrogen bonds between amino group of 4-atrz ligand and O atoms of POM {N(5)–H(5A)···O(16) and N(6)–H(6A)···O(3)} were shown in Fig. S3 (Supporting information). And the corresponding hydrogen bonding distances and angles were given in Table S3 (Supporting information).

The analysis of single crystal structure manifests that Cu^{2+} coordinates with 4-atrz, and then combines with PMo_{12} to form POMOC **1** through electrostatic interaction and hydrogen bonds. Therefore, the combination order of Cu^{2+} with 4-atrz affects the crystal size significantly, which is consistent with the above results of crystal size regulation. When Cu^{2+} interacts with 4-atrz first, it is beneficial for the faster construction of $\{Cu_3\}$ clusters to promote the formation of more POMOC **1** crystal nucleus and smaller POMOC **1** crystals. When Cu^{2+} reacts with CA to form chelate first, the coordination between Cu^{2+} and 4-atrz is inhibited, resulting in the formation of less crystal nucleus and POMOC **1**-SC with larger size. When Cu^{2+} reacts with PMo_{12} preferentially, the electrostatic interaction among them is easy to be destructed by the coordination between Cu^{2+} and 4-atrz. Therefore, the inhibition degree for nucleation is decreased, obtaining the middle size of POMOC **1** crystals. Furthermore, the structure analysis shows that there are no pores in POMOC **1**, thus only active sites exposed on crystal surface involve in catalysis. And nanoscale POMOC **1** crystals with larger specific surface area are in demand for the subsequent catalytic applications. However, the minimum size of POMOC **1** crystals prepared by the hydrothermal method at 120 °C was 4 μm under the feeding sequence of Cu^{2+}–4-atrz–PMo_{12}. In order to obtain smaller POMOC **1** crystals, the conventional synthesis at different reaction temperature from room temperature to 90 °C and a shorter reaction time of 30 min were carried out. The results showed that the crystal size of POMOC **1** prepared at 90 °C and 60 °C was obviously decreased but nonuniform (Figs. S4 and S5 in Supporting information). Finally, POMOC **1** with a crystal size of about 170 nm (denoted as **1**-Nano) was obtained after Cu^{2+}, 4-atrz and PMo_{12} stirring at room temperature for 30 min, as shown in Fig. 3a. The Powder X-ray diffraction (PXRD) patterns of POMOC **1** synthesized at above different conditions all matched well with that of the simulated by single-crystal data (Fig. 3b and Fig. S6 in Supporting information), indicating that all obtained POMOC **1** samples were pure phase.

The oxidation of phenols is a crucial reaction in the field of organic chemistry, in which the products of benzoquinones are essential intermediates for pharmaceuticals, dyes, fine chemicals and so on [39–41]. Especially, 2,3,5-trimethylbenzoquinone (TMBQ) is a key intermediate in the synthesis of vitamin E [42,43], which can be synthesized by oxidizing either 2,3,5-trimethylphenol (2,3,5-TMP) or 2,3,6-trimethylphenol (2,3,6-TMP) [44–46]. The oxidation reaction of 2,3,6-TMP to TMBQ with H_2O_2 as oxidant was used as the model reaction to evaluate the catalytic activity of POMOC **1**-Nano. In order to confirm the optimized reaction conditions, the effects of solvent, temperature, amount of catalyst and oxidant, and reaction time were investigated (Table S4 in Supporting information). Firstly, the influence of solvent was explored by adding 2,3,6-TMP (0.25 mmol), H_2O_2 (1 mmol), and POMOC **1**-Nano (8 μmol) as the catalyst into several different commonly used solvents (1 mL) and reacting at 60 °C for 2 min. When DMF, H_2O, dichloromethane and dichloroethane were severally used as the solvent, the oxidation of 2,3,6-TMP was negligible (<10%, Table S4, entries 1-4). 34% conversion and 73% selectivity of TMBQ were observed in the solvent of EtOH (Table S4, entry 5). MeCN was the optimum solvent, in which the conversion increased to 85% and the selectivity of TMBQ increased to 94% (Table S4, entry 6). Subsequently, the influence of temperature on the reactivity was explored in MeCN. When the reaction temperature was decreased from 60 °C to 50 °C, the conversion of 2,3,6-TMP reduced to 76% (Table S4, entry 7). When the temperature rose to 70 °C, the conversion of 2,3,6-TMP was also decreased to 79% (Table S4, entry 8), which may be owing to the faster decomposition of H_2O_2 at higher temperature. Then the optimum amount of catalyst was researched at 60 °C in MeCN. The results showed that the conversion of 2,3,6-TMP (85% *vs.* 78%) and selectivity of TMBQ (94% *vs.* 83%) were reduced when the amount of catalyst decreased from 8 μmol to 7 μmol (Table S4, entry 9). However, when the amount of catalyst was increased to 9 μmol, the conversion and selectivity dropped to 75% and 92%, respectively (Table S4, entry 10), which may be caused by the aggregation of POMOC **1**-Nano particles with small size. Next, the effect of the oxidant dosage on the catalytic reaction was investigated with a catalyst amount of 8 μmol. It was found that the conversion of 2,3,6-TMP was increased from 85% to 99% with the increase of the oxidant dosage from 1 mmol to 2 mmol, while the selectivity of TMBQ decreased from 94% to 86% (Table S4, entries 6, 11 and 12). Considering the yield of TMBQ comprehensively, 1.5 mmol of oxidant is optimum, which showed a conversion of 95% and a selectivity of 92%. Finally, the catalytic effect over the reaction time exhibited that the conversion increased significantly (53% to 95%) and the selectivity improved slightly (90% to 92%) within 2 min (Table S4, entries 6, 13−15). When the time was further extended, the conversion and selectivity were unchanged (Table S4, entries 16 and 17). In summary, POMOC **1**-Nano presented the best catalytic effect (95% conversion of 2,3,6-TMP and 92% selectivity of TMBQ) under a molar ratio of 1:6:0.032 for 2,3,6-TMP, H_2O_2 and catalyst at 60 °C within 2 min.

To estimate the universality of POMOC **1**-Nano for the oxidation reaction of phenols, phenols with different substituents were used as the reaction substrates (Table 1). The results showed that the conversion of methyl (electron-donating group) substituted phenols was over 80% and the selectivity of corresponding *p*-BQs was

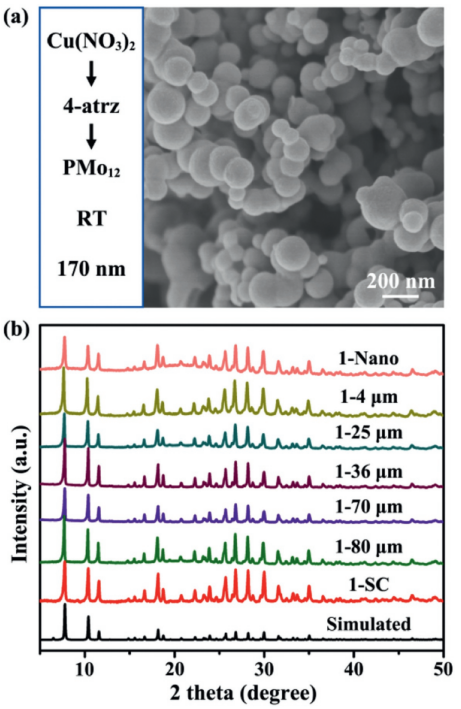
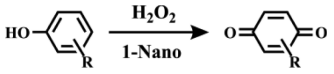
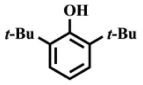
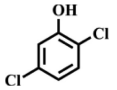


Fig. 3. (a) SEM image of POMOC **1**-Nano synthesized at room temperature. (b) PXRD patterns of the synthesized POMOC **1** with different sizes.

Table 1
The catalytic activity of POMOC 1-Nano for the oxidation reaction of phenols with different substituents.



Entry	Substrate	Time (min)	Con. (%)[c]	Sel. (%)[d]
1[a]		2	95	92
2[b]		30	91	91
3[b]		60	89	95
4[b]		60	84	96
5[b]		60	77	99
6[b]		60	13	98

[a] Reaction conditions: 0.25 mmol of substrate, 8 μmol of catalyst, 1 mL of MeCN, 1.5 mmol of H_2O_2, 60 °C.
[b] The dosage of H_2O_2 was 3 mmol.
[c] The conversion of the substrates was calculated using biphenyl as the internal standard and monitored by GC.
[d] Selectivity for target product.

over 90% (Table 1, entries 1-4). Even for alkyl substituted phenol with large steric hindrance, POMOC **1**-Nano also exhibited satisfying catalytic effect. For example, the conversion of 2,6-di–*tert*-butylphenol can reach to 77%, and the selectivity of corresponding *p*-BQ product reached to 99% (Table 1, entry 5). However, the conversion of dichlorophenol was poor (13%), due to the strong electron-absorbing effect of Cl group (Table 1, entry 6). These results indicated that POMOC **1**-Nano is an excellent catalyst candidate for the oxidation reaction of phenols with electron-donating groups.

In order to determine the catalytically active components in POMOC **1**-Nano catalyst for the oxidation reaction of phenols, the catalytic effects of different components were compared under the above optimized condition of 2,3,6-TMP oxidation reaction (Fig. 4a). Firstly, the conversion of 2,3,6-TMP was negligible (5%) under the condition of non-catalyst, suggesting the facilitation of POMOC **1**-Nano catalyst for 2,3,6-TMP oxidation reaction. Subsequently, $Cu(NO_3)_2$, PMo_{12} and 4-atrz were as the catalyst to be introduced into 2,3,6-TMP oxidation reaction, respectively. Among them, $Cu(NO_3)_2$ possessed higher catalytic activity, exhibiting a conversion of 58% and selectivity of 97%. The catalytic activity of PMo_{12} was secondary with 23% conversion and 83% selectivity, while 4-atrz was non catalytically active (conversion of 6% and selectivity of 96%) for 2,3,6-TMP oxidation reaction. Then the mechanical mixture of $Cu(NO_3)_2$, PMo_{12} and 4-atrz showed a conversion of 75% and selectivity of 70%, which were significantly lower than that of POMOC **1**-Nano (95% conversion and 92% selectivity). The above results indicated that coordinatively unsaturated Cu(II) sites and PMo_{12} sites in POMOC **1**-Nano play a synergistic catalysis for the oxidation of 2,3,6-TMP. Finally, the catalytic effects of POMOC **1** with different sizes for 2,3,6-TMP oxidation reaction were explored under the same conditions (Fig. 4b). As expected, the conversion of 2,3,6-TMP (29% to 95%) and the selectivity of TMBQ (57% to 92%) were both increased significantly with the decrease of POMOC **1** size from single crystal of 120 μm to nanocrystal of 170 nm. These results fully proved that nanocrystallization is an effective strategy to improve the catalytic effect of POMOCs without pores, due to more accessible active sites on the surface of nanocatalysts.

Based on the above analysis, it can be found that the excellent catalysis of POMOC **1**-Nano was originated from the synergistic effect of coordinatively unsaturated Cu(II) and PMo_{12} catalytic sites on the large surface of nano catalyst. And the detailed catalytic mechanism of these Cu(II) and PMo_{12} sites for the oxidation reaction of 2,3,6-TMP was investigated subsequently (Fig. S7 in Supporting information). Firstly, 2,6-di–*tert*–butyl–4-methylphenol (BHT) and 2,2,6,6-tetramethylpiperidin-1-yl)oxyl (TEMPO) separately as typical carbon free radical and oxygen free radical scavenger were added into the catalytic reaction system [47]. And the conversion of 2,3,6-TMP was decreased from 95% to 30% and 34%, respectively. Then 1,4-benzoquinone (*p*-BQ) and isopropyl alcohol (IPA) were used to individually quench $^{\bullet}O_2H$ and $^{\bullet}OH$, which are possible reactive oxygen species generated by H_2O_2 [48]. The conversion of 2,3,6-TMP was inhibited to 39% and 29% when *p*-BQ and IPA were presented, respectively. When both *p*-BQ and IPA were present, there was still 25% conversion of 2,3,6-TMP. Combining the above results and literature reports, it was speculated that there were two reaction pathways: (1) Cu(II) atom in the catalyst activated H_2O_2 to form $^{\bullet}O_2H$ and $^{\bullet}OH$, achieving the oxidation of 2,3,6-TMP through a free radical pathway [43]; (2) PMo_{12} was oxidized to peroxo-PMo_{12} by H_2O_2, which catalyzed the reaction through a non-free radical pathway [49]. The detailed conversion process of 2,3,6-TMP catalyzed by Cu(II) site (pathway A) and PMo_{12} site (pathway B) was showed in Fig. S8 (Supporting information). In pathway A, H_2O_2 was adsorbed and activated by Cu(II) atom to generate $^{\bullet}O_2H$, and then the reduced Cu(I) reacted with H_2O_2 to form $^{\bullet}OH$ while Cu(I) recovered to the initial Cu(II). Subsequently, $^{\bullet}OH$ abstracted H atom from the hydroxyl group of 2,3,6-TMP to produce a phenoxyl radical intermediate (A1). A1 was unstable and more likely to rearrange into a carbon radical intermediate (A2). Then A2 reacted with $^{\bullet}O_2H$ to form an unstable peroxyquinone intermediate (A3), which rapidly converted to the final product by losing one water molecule. In pathway B, PMo_{12} was oxidized by H_2O_2 to form highly active peroxo-PMo_{12}. Subsequently, the *para*-C atom of 2,3,6-TMP was subjected to electrophilic attack by peroxo-PMo_{12}, resulting in the heterolysis of C—H bond to form an active intermediate (B1). Then B1 was rapidly converted to 2,3,5-trimethylhydroquinone (B2) and the initial PMo_{12} site was obtained. Finally, B2 was further oxidized to TMBQ by another peroxo-PMo_{12}.

The recyclability and stability of catalysts are important indicators to evaluate the application of heterogeneous catalysts. The hot filtration experiment of 2,3,6-TMP oxidation reaction was carried out by removing POMOC **1**-Nano catalyst after 0.5 min of reaction, and then the filtrate was continued to react for 2 min at 60 °C. The conversion of 2,3,6-TMP was almost unchanged (Fig. 4c), demonstrating the heterogeneous catalysis and stability of POMOC **1**-Nano. To investigate the recyclability of POMOC **1**-Nano, the catalyst was recycled by centrifugation and washed with MeCN after reaction, which was reused for next run reaction after drying. As shown in Fig. 4d, there was no significant decrease for the conversion of 2,3,6-TMP after 5 cycles. The selectivity of TMBQ was decreased to 81% in the third cycle and then maintained, which may be due to the agglomeration of POMOC **1**-Nano particles in the process of recycling and drying (Fig. 4e) [50,51]. PXRD pattern and IR spectrum of recycled catalyst were consistent with that of the fresh (Fig. 4f and Fig. S9 in Supporting information), indicating the structure stability of POMOC **1**-Nano in the catalytic oxidation reaction of 2,3,6-TMP. All these results indicated the high recycla-

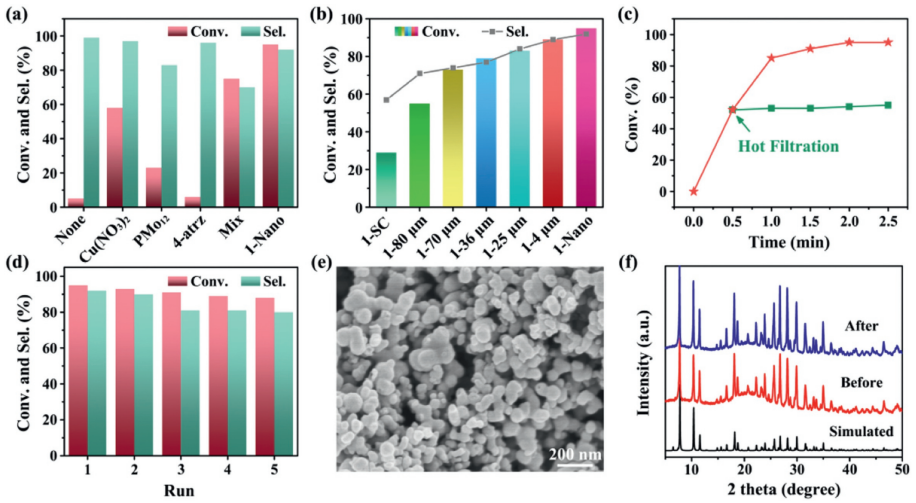


Fig. 4. Catalytic effect of (a) different components in POMOC **1** and (b) POMOC **1** with different crystal size on 2,3,6-TMP oxidation reaction. (c) Hot filtration and (d) recycling test of POMOC **1**-Nano catalyst for 2,3,6-TMP oxidation reaction. (e) SEM image and (f) PXRD patterns of POMOC **1**-Nano after catalysis.

bility and stability of POMOC **1**-Nano catalyst for the oxidation reaction of 2,3,6-TMP.

In summary, a new POMOC **1** composed of Cu(II), 4-atrz and PMo_{12} was synthesized in this work. The size regulation of POMOC **1** from 4 μm to single-crystal was achieved by introducing CA as a modulator under hydrothermal conditions. And nanoscale POMOC **1** with a size of 170 nm was obtained by simply stirring raw materials at room temperature. The single-crystal data analysis indicated that POMOC **1** presented a zero-dimensional structure. And POMOC **1** was constructed by the electrostatic interaction and hydrogen bonds between PMo_{12} and coordinatively unsaturated three-nucleated copper cluster. Nano-sized POMOC **1** can serve as an excellent heterogeneous catalyst for the oxidation reaction of phenolic compounds to quinones, due to the larger surface area and more utilizable active sites of the nano-catalyst. The conversion of 2,3,6-TMP and the selectivity of TMBQ separately reached 95 % and 92 % within 2 min at 60 °C under the synergistic catalysis of coordinatively unsaturated Cu(II) and PMo_{12} in nano-sized POMOC **1**. This work has achieved the size regulation of complicated-system POMOC containing triazole ligand, proposing a feasible approach for the broader application of such materials.

Declaration of competing interest

The authors declare that they have no known competing financial interests or personal relationships that could have appeared to influence the work reported in this paper.

CRediT authorship contribution statement

Yang Chu: Writing – original draft, Investigation. **Xiao-Hui Li:** Writing – review & editing, Funding acquisition. **Zhong Zhang:** Data curation. **Na Xu:** Methodology. **Dan-Feng He:** Investigation. **Xiu-Li Wang:** Writing – review & editing, Funding acquisition.

Acknowledgments

This work was financially supported by the National Natural Science Foundation of China (Nos. 22201021, 22271021, 22266028), the Doctoral Scientific Research Foundation of Liaoning Province (2022-BS-302), and the Natural Science Foundation and Education Department of Liaoning Province (No. LJ232410167011).

Supplementary materials

Supplementary material associated with this article can be found, in the online version, at doi:10.1016/j.cclet.2025.111012.

References

[1] W. An, X. Zhang, J. Niu, Y. Ma, Z. Han, Chin. Chem. Lett. 33 (2022) 4400–4404.
[2] H.X. Bi, M.S. Guo, J. Du, Y.Y. Ma, Z.G. Han, Coord. Chem. Rev. 518 (2024) 216092.
[3] H. Song, M.S. Guo, J.F. Wang, et al., Polyoxometalates 3 (2024) 9140065.
[4] Q. Wang, J. Wang, D. Zhang, et al., Polyoxometalates 3 (2024) 9140064.
[5] J.Y. He, J.F. Wang, J. Du, Y.Y. Ma, Z.G. Han, Eur. J. Inorg. Chem. 28 (2025) e202400584.
[6] X.Y. Yin, H.X. Bi, H. Song, et al., Polyoxometalates 2 (2023) 9140027.
[7] Y.N. Gong, J.H. Mei, W.J. Shi, et al., Angew. Chem. Int. Ed. 63 (2024) e202318735.
[8] Y.N. Gong, S.Y. Lv, H.Y. Yang, et al., CCS Chem. 6 (2024) 3030–3040.
[9] S. Zhang, B. Wang, S. Li, et al., J. Mol. Struct. 1297 (2024) 136929.
[10] Y.Y. Li, X.H. Li, Z.X. An, Y. Chu, X.L. Wang, Chin. Chem. Lett. 36 (2025) 109716.
[11] L. Yang, Z. Zhang, C.N. Zhang, X.L. Wang, Rare Met. 43 (2024) 236–246.
[12] P. Koley, S.C. Shit, T. Yoshida, et al., ACS Catal. 13 (2023) 6076–6092.
[13] S. Li, J. Sun, G. Liu, S. Zhang, Z. Zhang, X. Wang, Chin. Chem. Lett. 35 (2024) 109148.
[14] S. Li, M.Y. Huang, W. Cheng, et al., Inorg. Chem. Front. 11 (2024) 7324–7332.
[15] Y. Wang, Q. Liu, Y.Y. Ma, et al., Mol. Catal. 569 (2024) 114579.
[16] S. Li, Y. Zheng, G.C. Liu, X.H. Li, Z. Zhang, X.L. Wang, Polyoxometalates 3 (2024) 9140061.
[17] X.X. Li, L. Zhang, L. Yuan, et al., Chem. Engin. J. 442 (2022) 136157.
[18] T.Y. Dang, R.H. Li, H.R. Tian, et al., J. Mater. Chem. A 10 (2022) 16514–16523.
[19] S. Xing, J. Li, G. Niu, et al., Mol. Catal. 458 (2018) 83–88.
[20] Z. Li, Z.H. Lv, H. Yu, et al., CCS Chem. 4 (2022) 2938–2945.
[21] Y.Y. Ma, H.Q. Tan, Y.H. Wang, et al., CrystEngComm 17 (2015) 7938–7947.
[22] F. Li, J. Li, L. Zhou, S. Dai, Sustain. Energ. Fuels 5 (2021) 1095–1102.
[23] N. Geng, F. Wang, D. He, et al., Fuel 341 (2023) 127021.
[24] J. Park, Q. Jiang, D. Feng, L. Mao, H.C. Zhou, J. Am. Chem. Soc. 138 (2016) 3518–3525.
[25] X. Sui, X. Huang, H. Pu, Y. Wang, J. Chen, Nano Energy 83 (2021) 105797.
[26] S. Hermes, T. Witte, T. Hikov, et al., J. Am. Chem. Soc. 129 (2007) 5324–5325.
[27] S. Yuan, M. Weng, D. Liu, et al., ACS Sustain. Chem. Eng. 7 (2019) 18912–18925.
[28] L. Chen, Z. Li, Y. Dou, et al., J. Hazard. Mater. 469 (2024) 134045.
[29] J. González, P. Sevilla, G. Gabarró-Riera, et al., Angew. Chem. Int. Ed. 60 (2021) 12001–12006.
[30] H. Li, M. Liang, W. Sun, Y. Wang, Adv. Funct. Mater. 26 (2016) 1098–1103.
[31] F. Bigdeli, M.N.A. Fetzer, B. Nis, A. Morsali, C. Janiak, J. Mater. Chem. A 11 (2023) 22105–22131.
[32] T. Uemura, Y. Hoshino, S. Kitagawa, K. Yoshida, S. Isoda, Chem. Mater. 18 (2006) 992–995.
[33] H. Zhou, L. Zhang, G. Wang, et al., ACS Appl. Mater. Interfaces 13 (2021) 39755–39762.
[34] T. Tsuruoka, S. Furukawa, Y. Takashima, et al., Angew. Chem. Int. Ed. 48 (2009) 4739–4743.
[35] H.Z. Li, S. Li, F. Wang, J. Zhang, Inorg. Chem. Front. 11 (2024) 2876–2883.
[36] M. Maxeiner, L. Wittig, A.E. Sedykh, T. Kasper, K. Müller-Buschbaum, J. Mater. Chem. A 11 (2023) 22478–22491.
[37] Y. Liu, S. Liu, D. He, et al., J. Am. Chem. Soc. 137 (2015) 12697–12703.
[38] X.L. Wang, C.H. Gong, J.W. Zhang, et al., CrystEngComm 17 (2015) 4179–4189.

[39] L. Que, W.B. Tolman, Nature 455 (2008) 333–340.
[40] W. Ye, X. Shi, Y. Zhang, et al., ACS Appl. Mater. Interfaces 8 (2016) 2994–3002.
[41] E.T. Saka, Y. Çağlar, Catal. Lett. 147 (2017) 1471–1477.
[42] M. Eggersdorfer, D. Laudert, U. Létinois, et al., Angew. Chem. Int. Ed. 51 (2012) 12960–12990.
[43] O.A. Kholdeeva, O.V. Zalomaeva, Coord. Chem. Rev. 306 (2016) 302–330.
[44] Y. Li, P. Zhang, M. Wu, W. Liu, et al., Chem. Eng. J. 146 (2009) 270–274.
[45] V.Yu. Evtushok, A.N. Suboch, O. Yu, et al., ACS Catal. 8 (2018) 1297–1307.
[46] S. Chang, Y. Chen, H. An, et al., Green Chem. 23 (2021) 8591–8603.
[47] Y. Li, X. Li, Z. An, Y. Chu, X. Wang, Chem. Asian J. 18 (2023) e202300814.
[48] J. Yang, L. Li, C. Xiao, Y. Xie, Angew. Chem. Int. Ed. 62 (2023) e202311911.
[49] Y. Lin, B. Li, Z. Feng, et al., ACS Catal. 5 (2015) 5921–5926.
[50] Y.Y. Li, X.H. Li, N. Xu, et al., Mol. Catal. 548 (2023) 113428.
[51] W. Subramonian, T.Y. Wu, S.P. Chai, J. Environ. Manage. 187 (2017) 298–310.